Quantitative imaging of large-scale structures and molecular mixing in gaseous free shear flows

T. R. Meyer,[*] G. F. King,[**] G. C. Martin,[*] R. P. Lucht,[†] F. R. Schauer,[‡] and J. C. Dutton[*]

[*] University of Illinois, Urbana, IL 61801, USA
[**] 3M Corporation, St. Paul, MN 55144, USA
[†] Texas A&M University, College Station, TX 77843, USA
[‡] Air Force Research Laboratory, Wright-Patterson AFB, OH 45433, USA

ABSTRACT

Previous investigations have demonstrated that it is possible to obtain quantitative images of subresolution molecular mixing in free shear flows using chemically reactive tracer species. The advantage of such techniques over highly-resolved measurements is their ability to obtain molecular mixing data over the entire flowfield, and as such, to study the effects of large-scale motions on molecular mixing. In gaseous flows, this has been accomplished using simultaneous cold-chemistry (nitric oxide) and passive scalar (acetone) planar laser-induced fluorescence. The current work summarizes the theoretical and experimental bases for this technique, discusses the unique advantages of using simultaneous tracers, and analyzes various sources of error and uncertainty that can degrade quantitative accuracy. Such errors can result from the use of nitric oxide quenching corrections, differential diffusion of tracer species, and finite imaging spatial resolution. Results from experimental measurements are presented in conjunction with a direct numerical simulation of species transport in a driven axisymmetric jet.

1. INTRODUCTION

The effect of large-scale structures on localized molecular mixing and chemical reaction rates is of considerable interest in the combustion and chemical processing communities. Planar laser-induced fluorescence (PLIF) has been used extensively to image the scalar field in both reacting and non-reacting flows, and a variety of laser-based techniques have been implemented, such as three-dimensional (Hanson 1986), multispecies (Yip, et al. 1994, Seitzman, et al. 1994), and high resolution (Dahm, et al. 1991, Su and Clemens 1998) measurements. In most experiments with high-speed flows, however, one must choose to image either the large-scale structures or the finest mixing scales, but not both. An exception is in the acid-base chemical product visualizations of liquid mixing first used by Breidenthal (1981) and extended for use with PLIF by Koochesfahani et al. (1985). Because of the considerable difference in Schmidt numbers between liquids and gases, however, an analogous technique for gaseous flows is required.

Such a technique for gas phase measurements of molecular mixing in low-speed flows has been proposed by Yip, et al. (1994) using sensitized phosphorescence. For high-speed flows, simultaneous imaging of large-scale structures and molecular unmixedness has been achieved by using the so-called cold-chemistry (fast-quenching) behavior of nitric oxide (NO) fluorescence in the presence of oxygen (Paul and Clemens 1993, Clemens and Paul 1995). While mixing statistics can be obtained on a time-averaged basis using a flip experiment (Island, et al. 1996), the obvious limitation of this technique is that it cannot be used to obtain instantaneous images of molecular mixing.

The first technique to measure instantaneous molecularly mixed fluid quantities while simultaneously visualizing the large-scale structures in high-speed gaseous shear flows was implemented by King, et al. (1997). This technique uses acetone PLIF as a passive-scalar measurement of the fluid fractions from each fluid stream of a shear layer, and uses NO PLIF simultaneously to obtain the molecularly unmixed fluid fraction. Thus, the instantaneous molecularly mixed fluid fraction, mixing efficiency, and relevant statistics can be obtained in post-processing. A number of studies in driven jets and high-speed turbulent jets have been performed using this approach (King, et al. 1999, Meyer, et al. 1999a,b), and measurements are currently underway in a planar shear layer facility. In this paper, the

capabilities and limitations of the technique are discussed from the standpoint of acquiring quantitative results, and as a means of performing basic research on turbulent mixing. As a necessary step to understanding and avoiding

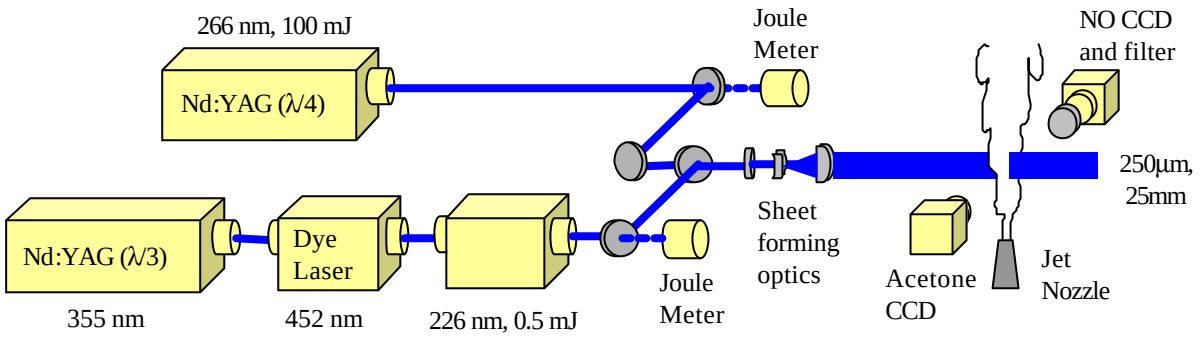

Figure 1: Simultaneous NO and acetone PLIF lasers and optics.

possible sources of uncertainty, we begin with an overview of experimental considerations, dual-tracer PLIF theory, and image processing procedures. More advanced considerations, such as the implementation of finite quenching rate corrections for NO fluorescence, are then discussed. Differential diffusion of air and acetone with nitrogen, which limits the ability of acetone to act as an accurate tracer for air, is evaluated and compared with results from a direct numerical simulation (DNS). Finally, errors due to finite resolution are assessed in the context of making *resolution free* measurements of molecular mixing.

2. EXPERIMENTAL SET-UP

The experimental set-up for dual-tracer PLIF is discussed by King et al. (1997, 1999) and Meyer et al. (1999a), and is summarized here for reference. The typical set-up for simultaneous NO and acetone PLIF lasers and optics is shown in Fig. 1. The excitation spectrum for acetone ranges from 225 to 325 nm, with a peak at 275 nm. Thus, acetone excitation was achieved using a frequency quadrupled Nd:YAG laser, which produced a 266 nm beam with pulse energies of about 100 mJ. The excitation spectrum for NO has discrete peaks corresponding to various rotational transitions. Excitation of the NO γ-band $Q_1(1)$-$Q_1(4)$ transitions centered at about 226.185 nm wavelength was achieved using the frequency doubled output of a Nd:YAG-pumped dye laser, with final pulse energies of about 0.5 mJ. The two beams were combined using a dichroic mirror, then formed into a sheet that was 25 mm in height and 250 μm thick. In current experiments, pyroelectric joule meters are used to measure both beam energies simultaneously with each camera exposure event. This is useful during post-processing for distinguishing between the temporal variation of beam energy with that of seeding density in the PLIF images. Knowledge of the relative image-to-image beam energy is useful in laser sheet profile corrections, and knowledge of the seeding density improves the accuracy of NO quenching corrections.

The jet fluid consisted of nitrogen seeded at 200-300 ppm NO, and the co-flow air was seeded at 4.6% acetone by mass. Note that the nitrogen was selected as the carrier fluid for NO because its quenching cross-section is at least three orders of magnitude smaller than that of oxygen. As the carrier fluid for acetone, air served not only to quench NO fluorescence upon molecular mixing, but also quenches any acetone phosphorescence. The signal from acetone PLIF ranges from 300 to 700 nm, with a peak at about 450 nm. It was collected using a 512x512 CCD camera equipped with a 1.2 f# glass lens, and is capable of 42% quantum efficiency at 450 nm. The glass lens filtered stray UV light from both incoming laser beams, and filtered the UV fluorescence from the NO PLIF signal. The signal from the NO PLIF consists of discrete wavelengths ranging from 225 to 300 nm. It was collected with an identical 512x512 CCD camera equipped with a 4.5 f# multielement UV lens, and is capable of 15% quantum efficiency at 240 nm. No UV filters were used to remove scatter from the incoming laser beams, although repeatable scatter was removed via background subtraction in post-processing. The lower quantum efficiency and higher f# of the NO camera helped to

minimize the visible acetone fluorescence collected by the NO camera. Earlier experiments did not use a filter to prevent the NO camera from collecting visible acetone fluorescence. In subsequent experiments, a filter was used in

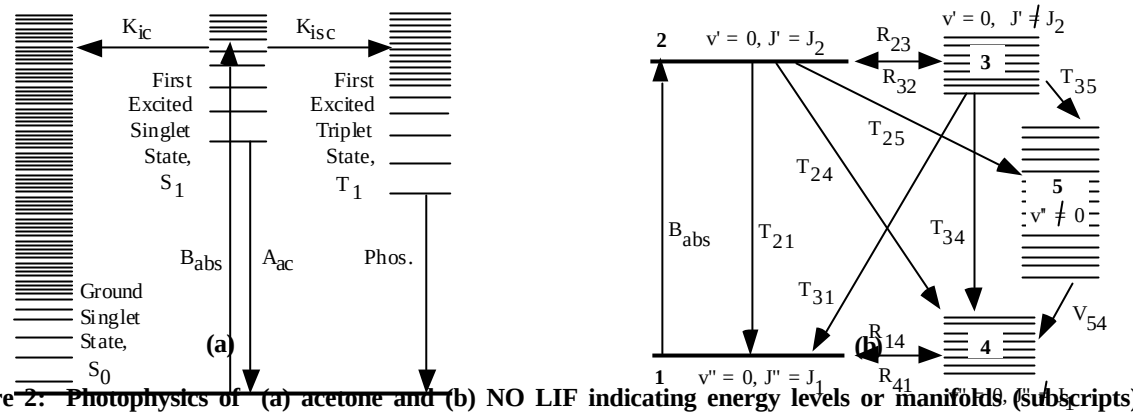

Figure 2: Photophysics of (a) acetone and (b) NO LIF indicating energy levels or manifolds (subscripts), and relevant transfer meachanisms (A – spontaneous emission, B – stimulated absorption, K – internal transfer, R – rotational transfer, T – spontaneous emission + collisional quenching, V- vibrational transfer).

front of the UV camera in order to reduce the residual acetone signal by about 50%.

3. DUAL-TRACER PLIF THEORY

For a given imaging system with uniform laser intensity, weak laser excitation (linear regime), frozen rotational manifolds (two−level model), and constant overall number density, the PLIF signal, $S_{f,i}$ from each seeded fluid, i, is proportional to the mole fraction of seeded fluid, x_i, and the fluorescence efficiency (Eckbreth 1988).

$$S_{f,i} \approx x_i \frac{A_i}{A_i + Q_i + K_i} \tag{1}$$

The local fluorescence efficiency is proportional to the rate of spontaneous emission, A_i, from molecules in the excited state, and inversely proportional to the rate at which excited molecules are depleted via spontaneous emission, A_i, collisional quenching, Q_i, and internal decay, K_i. The determination of molecularly mixed fluid quantities using simultaneous NO and acetone PLIF is made possible by the disparate fluorescence efficiencies of these tracers after molecular mixing has taken place (King, et al. 1997).

A detailed discussion of acetone LIF can be found in a number of references (Hansen and Lee 1975, Lozano, et al. 1992). Figure 1(a) shows a simple model of acetone photophysics involving three relevant electronic states. Acetone molecules are excited by stimulated absorption at a rate B_{abs} from the ground singlet state, S_o, to the first excited singlet state, S_1. Rapid intersystem crossing then occurs from S_1 to the first excited triplet state, T_1, at a rate of K_{isc}, leaving only a small fraction of molecules in S_1 to fluoresce and decay back down to S_o. Phosphorescence from T_1 is highly quenched in the presence of oxygen, and is not a factor when acetone is seeded into air. Because of rapid intersystem crossing from S_1 to T_1, $K_{ac} = K_{isc} + K_{ic} >> A_{ac} + Q_{ac}$. Thus, K_{ac} dominates the denominator of Eq. 1, and the fluorescence efficiency of acetone becomes independent of the quenching environment. When the local fluorescence signal from the mixing layer (where $x_{ac} < 1$) is normalized to the signal from a pure region outside of the mixing layer (where $x_{ac} = 1$), the local mole fraction of acetone-seeded fluid, x_{ac}, can be found by:

$$x_{ac} = \frac{S_{f,ac}(mixing\ \ layer)}{S_{f,ac}(pure\ \ region)} = \frac{x_{ac} \times (A_{ac} / K_{ac})}{1 \times (A_{ac} / K_{ac})} \tag{2}$$

A five-level energy diagram for NO LIF is shown in Fig. 2(b). In this diagram, v" and J" are vibrational and rotational levels, respectively, in the ground electronic state ($X^2\Pi$), and v' and J' are vibrational and rotational levels, respectively, in the first excited electronic state ($A^2\Sigma$). In the limit of fast rotational energy transfer, however, this

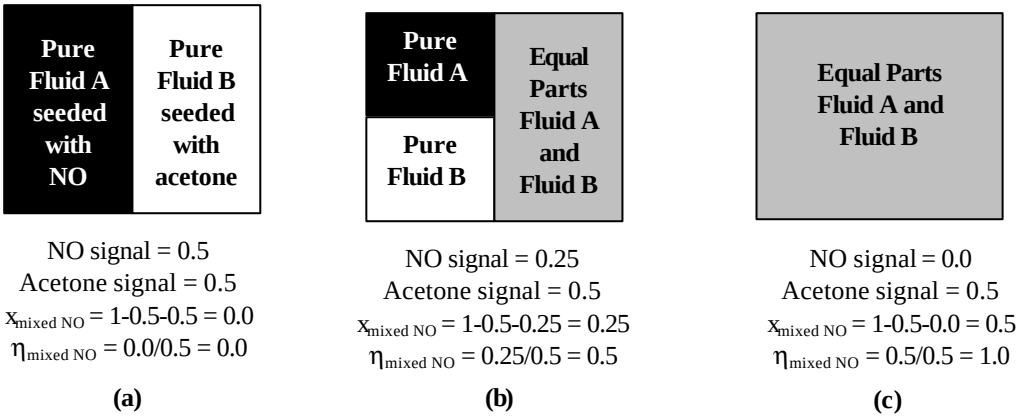

five-level model can be approximated with the two-level model from Eq. 1. Fluorescence is then collected from

Figure 3. Sample calculations illustrating the effects of subresolution stirring and mixing in a pixel with two different fluids in the (a) pure, (b) partially mixed, and (c) fully mixed states.

resonant fluorescence at the excitation wavelength (i.e., path 2-1) and nonresonant transfers with other rotational levels (e.g., paths 3-1 and 2-4). The transfer rate, T, includes both spontaneous emission, A, and collisional quenching, Q. The cold-chemistry limit assumes that quenching rates dominate spontaneous emission and internal decay rates ($Q_{NO} >> A_{NO} + K_{NO}$) and that the quenching rate when NO is mixed with acetone-in-air is much greater than the quenching rate when NO is in pure nitrogen ($Q_{mixed\ NO} >> Q_{pure\ NO}$). From these assumptions, the normalized fluorescence signal is a direct measure of the local mole fraction of *pure* NO-seeded fluid, $x_{pure\ NO}$. Using the same procedure as for Eq. 2 and noting that $x_{NO} = x_{pure\ NO} + x_{mixed\ NO}$, it follows that:

$$x_{pure\ NO} = \frac{S_{f,NO}(mixing\ \ layer)}{S_{f,NO}(pure\ \ region)} = \frac{x_{pure\ NO} \times \left(A_{NO} / Q_{pure\ NO}\right) + x_{mixed\ NO} \times \left(A_{NO} / Q_{mixed\ NO}\right)}{1 \times \left(A_{NO} / Q_{pure\ NO}\right)} \tag{3}$$

In a binary mixture, the mole fraction of NO-seeded fluid, x_{NO}, is simply equal to 1-x_{ac}. The mole fraction of *molecularly mixed* NO-seeded fluid can then be found by:

$$x_{mixed\ NO} = x_{NO} - x_{pure\ NO} = 1 - x_{ac} - x_{pure\ NO} \tag{4}$$

Finally, a mixing efficiency can be defined as the ratio of molecularly mixed NO-seeded fluid to total NO-seeded fluid such that:

$$h_{mixed\ NO} = \frac{x_{mixed\ NO}}{x_{NO}} = \frac{x_{mixed\ NO}}{1 - x_{ac}} \tag{5}$$

The mixing efficiency is an important parameter in that values greater than zero and less than unity indicate that a pixel is composed of fluid from both fluid streams with at least some of the fluid being unmixed at the molecular level. Thus, the mixing efficiency can be used to identify regions in which subresolution stirring is takes place.

Figure 3(a)-(c) illustrates how the dual-tracer technique is able to obtain the mole fraction of mixed NO-seeded fluid as well as mixing efficiency on a pixel-by-pixel basis, and shows why a passive scalar tracer alone can lead to large errors in the measurement of molecularly mixed mole fractions. In case (a), equal parts of pure fluid from each fluid stream fill the pixel element. In case (b), some molecular mixing has taken place, but pure fluid regions still exist within the pixel. In case (c), the fluids in the pixel element are completely mixed. The normalized NO and acetone PLIF signals and the calculations of mixed NO-seeded fluid and mixing efficiency are shown below each corresponding pixel in Fig.

3. Note that the passive scalar acetone measurement alone can significantly overpredict the amount of mixed fluid, as in cases (a) and (b), since it cannot distinguish between the pure and mixed states within a pixel element. The dual-tracer PLIF technique, on the other hand, provides the correct amount of molecularly mixed NO-seeded fluid even though subresolution stirring is taking place in cases (a) and (b).

4. IMAGE PROCESSING

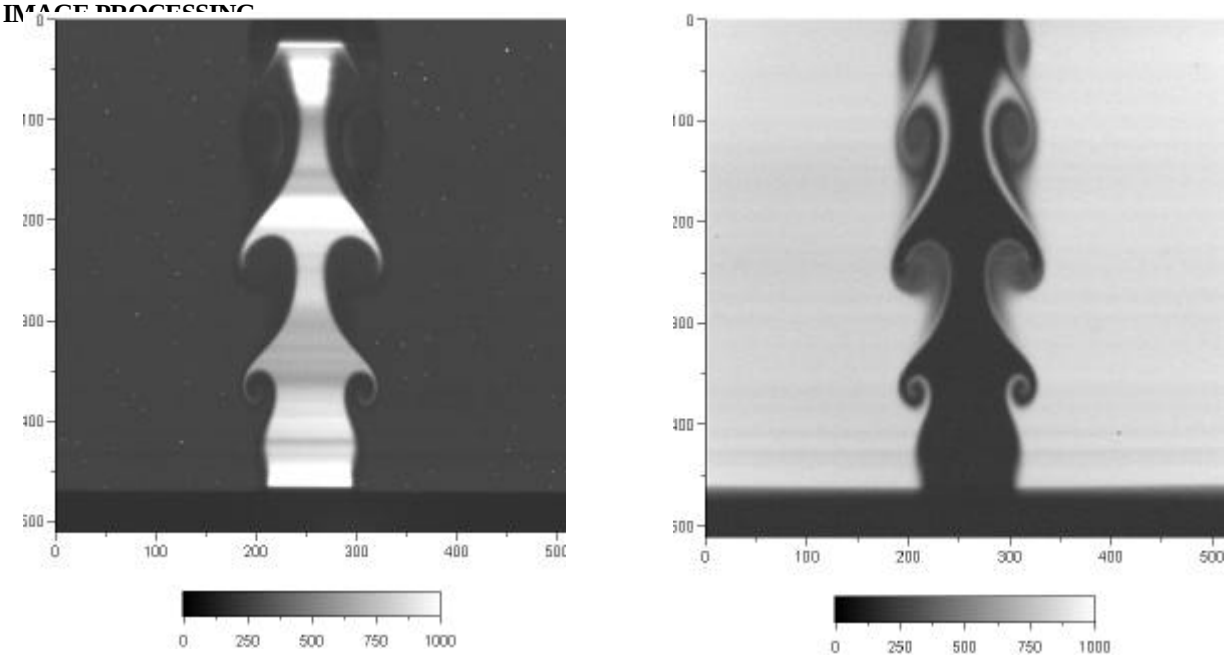

Figure 4. Simultaneous, raw images of (a) NO PLIF and (b) acetone PLIF. Spatial scales are in pixels and gray scales are in camera counts.

Image processing procedures for simultaneous visualization of NO and acetone PLIF have been summarized by King et al. (1997, 1999) and Meyer et al. (1999a). For example, Fig. 4 shows raw images of NO and acetone PLIF from the driven jet of Meyer et al. (1999a) at $Re_D = 2300$. Once the raw images have been obtained, the image processing procedures include image matching, background subtraction, attenuation correction, and laser sheet normalization. Note in both raw images of Fig. 4 that the laser sheet does not illuminate the entire camera viewing area, resulting in a dark "bar" at the bottom of each image. From this lower region in Fig. 4(a), it is clear that the CCD camera equipped with a UV lens collects a small amount of visible light (~5-7%) from the acetone signal. This residual acetone signal can be estimated from the acetone image in Fig. 4(b) and subtracted during post processing. While it is difficult to detect in Fig. 4(b), the signal from the center of the jet is higher than the unilluminated region at the bottom of the image due to Rayleigh scattering (~2%). This signal can also be subtracted during post-processing.

Figures 5(a) and (b) show the corrected images that result from the procedures discussed above. As stated previously, the normalized NO signal in Fig. 5(a) represents the fraction of *pure* NO-seeded jet fluid, $x_{pure\ NO}$, since NO fluorescence is almost entirely quenched when molecularly mixed with oxygen and acetone in the co-flow air. Thus, in the relatively laminar vortex rollers shown in the figure, where mixing is dominated by diffusion, one should expect very little NO signal. The fact that some signal is detected in the vortex rollers of Fig. 5(a) may result either because of errors when eliminating the residual acetone signal, or from the fact that NO fluorescence is not *completely* quenched in the presence of oxygen. The former can be reduced by adding an appropriate filter to the UV lens to block visible light, and the latter will be discussed further in the context of NO fluorescence quenching corrections.

Based on Eq. 2, t signal i he fracti ked co-flow fluid, x_{ac}, since acetone unquenc mixed. es from Figs. 5(a) and (b) can be us ction of fluid, as Note that the Mie scattering appar on of Fi during p oes not appear in Fig. 5(c).

5. QUENCHING

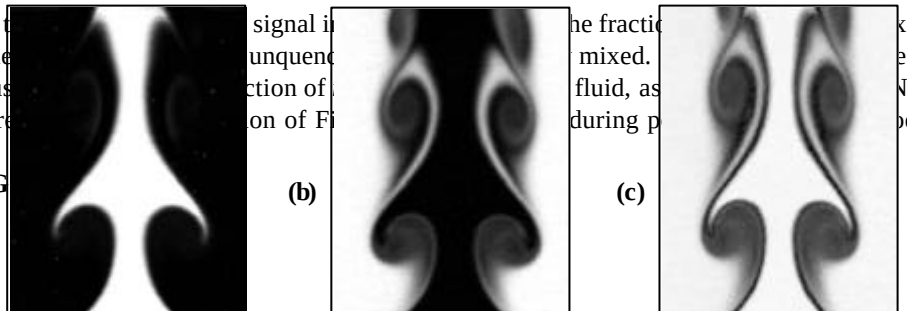

Figure 5. Post-processing images of (a) normalized NO PLIF, (b) normalized and remapped acetone PLIF, and (c) mixed jet fluid fraction. Gray scale is from 0 to 1.

As noted earlier, NO fluorescence is not completely quenched when mixed with only a small amount of air and acetone. More specifically, the assumptions that $Q_{NO} >> A_{NO} + K_{NO}$ and $Q_{mixed\ NO} >> Q_{pure\ NO}$ in Eq. 3 may not be completely valid. The rate of collisional quenching, Q_{NO}, at a co-flow mole fraction of 5%, for example, is only one order of magnitude greater than the rate of spontaneous emission, A_{NO}. The rate of collisional quenching, $Q_{mixed\ NO}$, at a co-flow mole fraction of 5% is also only an order of magnitude greater than the rate of collisional quenching, $Q_{pure\ NO}$, in the pure NO-seeded nitrogen jet. Thus, cold-chemistry errors are not insignificant in regions of low co-flow concentration.

One of the benefits of using simultaneous NO and acetone PLIF is that the fraction of air is known from the acetone signal, and this can be used to calculate the residual NO signal expected at low air concentrations. In previous investigations, for example, NO PLIF has been used to image the fraction of molecularly unmixed fluid. A flip experiment is then used to obtain statistics of unmixedness from both fluid streams, and thus obtain statistics of mixedness on a time-averaged basis. In one such study (Clemens and Paul 1995), significant "halo"regions of low NO signal (~10%) were reported adjacent to the regions of high NO signal. This is reminiscent of the residual NO signals shown in the vortex cores of Fig. 5(a). The authors of the study assumed, however, that the residual signal represented small amounts of pure NO-seeded fluid, which infers that subresolution stirring takes place. At low air concentrations, however, it is also possible that these "halo" regions were completely mixed, and that the residual signal resulted instead from the cold-chemistry error discussed above.

In order to quantify the expected residual signal at various co-flow fluid fractions, the quenching cross-sections, σ_i, of various relevant species have been calculated using correlations developed by Paul et al. (1994). The quenching rate, Q_i, for each species, i, can then be calculated from (Eckbreth 1988):

$$Q_i = x_i N_{tot} V_{i-NO} \sigma_i \tag{6}$$

where x_i is the mole fraction of species i, N_{tot} is the total number density as a function of temperature and pressure, and $V_{i\text{-}NO}$ is the average relative velocity between species i and NO. The total quenching rate is simply the sum of all the quenching rates for all the species present. By using the two-level model of Eq. 1, the expected normalized NO signal from Eq. 3 can be calculated as:

$$\frac{S_{f,NO}(mixing\ \ layer)}{S_{f,NO}(pure\ \ region)} = x_{NO}\frac{A_{NO} + Q_{pure\ NO}}{A_{NO} + Q_{mixed\ NO}} \tag{7}$$

(where x_{NO} is the total fraction of NO-seeded fluid equal to 1-x_{air}). The results from this model with NO-seeded in nitrogen at 300 ppm and air as [illegible] shown in Fig. 6(a). The results of a [illegible] on all of the transfer processes show [illegible]), is also shown in Fig. 6(a), and [illegible] assumption of fast rotational transfer is va[illegible] results, regions of 10% residual [illegible] for air mole fractions of about 8%. [illegible] completely quenched until the air mole fraction has reached about 20%.

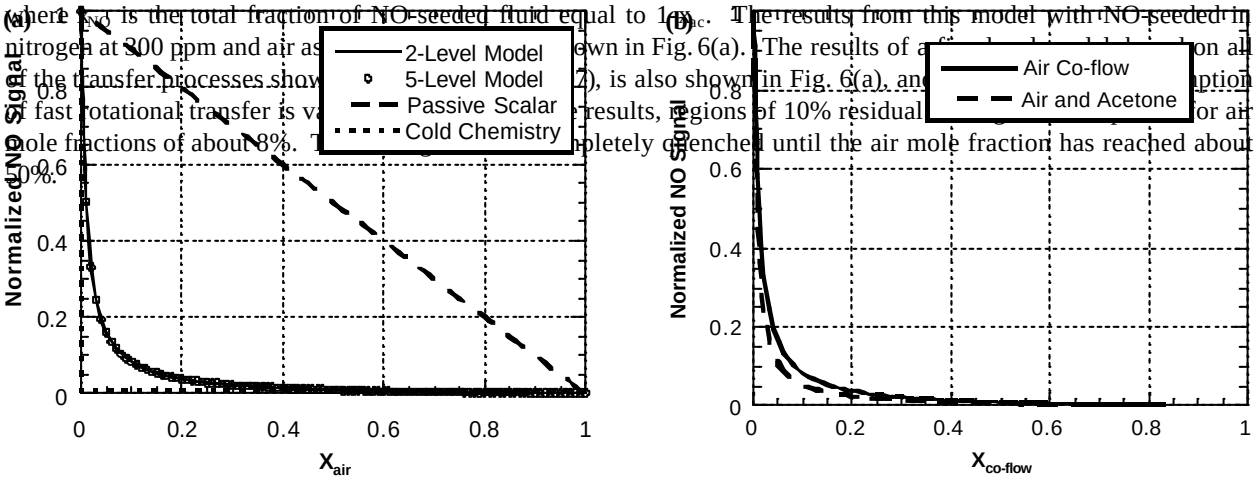

Figure 6. Plots of the normalized NO fluorescence signal as a function of the quenching environment for (a) various models and assumptions and (b) different co-flow fluids.

Fig. 6(b) shows that specific knowledge of the quenching environment can be fairly important. In the dual-tracer technique, for example, quenching due to acetone must also be considered. As shown in Fig. 6(b), the residual NO signal of 10% occurs at an acetone-in-air co-flow mole fraction of about 5% rather than the 8% for air alone. The NO seeding density can also have a significant effect on the quenching rate through the term $Q_{pure\ NO}$, since NO has a quenching cross-section that is almost four orders of magnitude larger than that of nitrogen.

Figure 6 clearly demonstrates that the NO signal is not completely quenched even when molecularly mixed with the co-flow fluid, and a correction should be included in the image processing procedures. Referring to Fig. 6(a), if a pixel element contained 50% co-flow air, then 50% would consist of the NO-seeded fluid. If all of this fluid was unmixed, then the passive scalar model would apply, and the expected normalized NO signal would be $x_{NO} = 50\%$. If all of the fluid was mixed, then the two-level model would apply, and an NO signal of $x_{NO,2\text{-}lev} = 1\%$ would be expected. If the pixel element was partially mixed, however, then the experimentally measured signal, $x_{NO,exp}$, would be somewhere between these values. A lever rule can then be used to determine $x_{mixed\ NO}$ as follows:

$$x_{mixed\ NO} = x_{NO}\frac{(x_{NO} - x_{NO,\exp})}{(x_{NO} - x_{NO,2-lev})} \tag{8}$$

Using the same example described above with 50% co-flow air, a sample calculation can be performed using the case of Fig. 3(b), in which some of the NO-seeded fluid is mixed and some is pure. The signal from the pure region would be 25%, and the signal from the mixed region would be 0.5%, such that $x_{NO,exp} = 25.5\%$. Using Eq. 8:

$$x_{mixed\ NO} = 0.5\frac{(0.5 - 0.255)}{(0.5 - 0.01)} = 0.25$$

Thus, the correct amount of mixed NO-seeded fluid is obtained. Note that the cold-chemistry model assumes that $x_{pure\ NO} = x_{NO,exp}$. Using this assumption in conjunction with Eq. 4 would lead to $x_{mixed\ NO} = 1 - x_{ac} - x_{pure\ NO} = 0.245$, or an

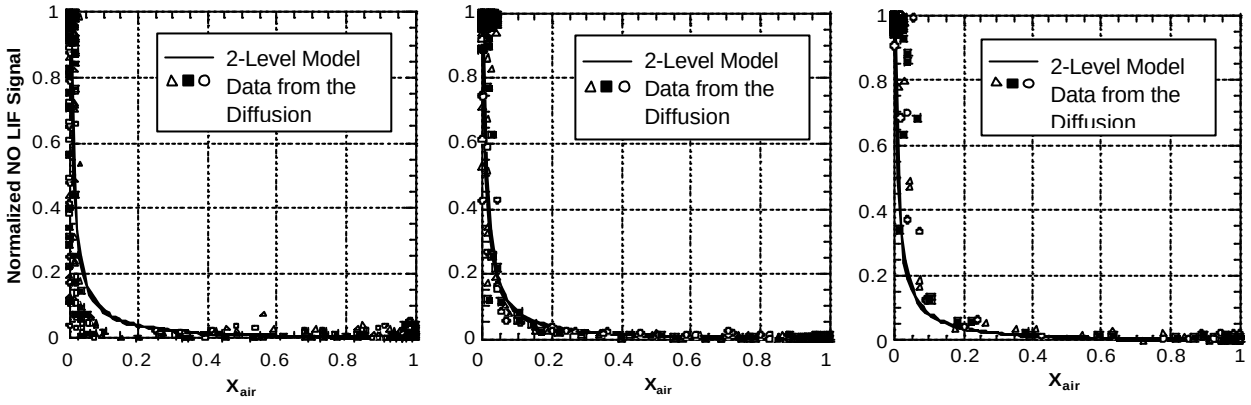

Figure 7. Plots of the normalized NO fluorescence signal as a function of co-flow air fraction from the two - level model compared with dual-tracer PLIF data from the laminar diffusion layer.

error of only 2%. Given a co-flow fraction of 5%, however, the cold-chemistry error can be as high as 10-20%.
In order to perform NO quenching corrections effectively, a number of factors should be considered. A low signal-to-noise ratio in the acetone images, for example, could lead to large errors in the corrected value of $x_{mixed\ NO}$ in regions of low air concentration. For this reason, it may be necessary to use a filtered data set of x_{ac} for the quenching corrections. Care must also be taken to avoid small errors in background subtraction and normalization, as these would further compound errors in the quenching corrections. A more subtle weakness is that the amount of NO

quenching is not directly a function of the measured fraction of co-flow fluid, x_{ac}. The reason for this is that x_{ac} contains both pure and mixed acetone-seeded fluid. If subresolution stirring of pure acetone-seeded fluid takes place within a pixel, then the amount of quenching may be overestimated. This weakness is offset, however, by the fact that quenching corrections are most dramatic in regions of low co-flow fluid concentration. In these regions, co-flow fluid should mix quickly and large pockets of pure co-flow fluid are unlikely to occur.

Another subtle difficulty is that the amount of mixed NO-seeded fluid is not known a priori. Take an example in which a pixel element consists of 80% pure NO-seeded fluid, 10% mixed NO-seeded fluid, and 10% mixed co-flow fluid. Based on Fig. 6, the residual NO signal with x_{ac} = 10% is predicted to be about 5%. In reality, the signal from the region of 10% mixed NO fluid will be reduced to 1% because the mixed region consists of equal parts NO-seeded fluid and acetone-seeded fluid. To avoid this error, an iterative procedure can be employed using Eq. 8:

$$\text{Step 1: } x_{mixed\ NO} = 0.9\frac{(0.9-0.802)}{(0.9-0.05)} = 0.104$$

$$\text{Step 2: } x_{mixed\ NO} = 0.9\frac{(0.9-0.802)}{(0.9-0.01)} = 0.099$$

Step 1 leads to an error of 5%. Once the fraction of mixed NO is estimated to be about 10.5%, however, then the fraction of co-flow fluid in the mixed region would be 10/(10+10.5) or 49%. In Step 2, $x_{NO,2\text{-}lev}$ = 0.01 was determined from Fig. 6 using a co-flow fluid fraction of 49% rather than 10%, leading to an error of only 1%.

6. DIFFERENTIAL DIFFUSION

It is clear that quenching corrections are important for avoiding potentially large cold-chemistry errors, and the steps outlined above can lead to a fair degree of confidence in their effectiveness. One of the unavoidable difficulties in using acetone as a tracer for air, however, is that air diffuses into N_2 at nearly twice the rate that acetone diffuses into N_2. As a result, a pixel element may contain more air than expected. The effect of this excess air is shown in the results of Fig. 7(a), where the measured NO signal is more highly quenched than expected. At higher Reynolds numbers, such as in Fig. 7(b), the width of the diffusion layer is expected to decrease, and the error from differential diffusion is reduced. In Fig. 7(c), the effects of finite resolution error, to be discussed later, become apparent.

In order to estimate the effects of differential diffusion, direct numerical simulations (DNS) of a steady 5 mm diameter axisymmetric jet were performed at Reynolds numbers of 1000 – 10,000, and in a pulsed configuration. The latter simulation was designed to mat[illegible] previous fluid tracer PLIF experiment ([illegible] with a time-averaged jet exit velocit[illegible]stic pulsing at 20 Hz. A variably space[illegible] 40 elements from r = 0 to 8 mm and 50 elements from x = 8 to 60 mm. The axial grid used 120 elem[illegible] mm and 30 elements from x = 60 to 100 mm. The grid density and domain size were varied to ensure that the results were grid independent and free of boundary effects. The numerical solver was originally developed for use in jet diffusion flames and is capable of momentum, energy, and multi-species transport calculations (Katta, et al. 1994a, b, and c).

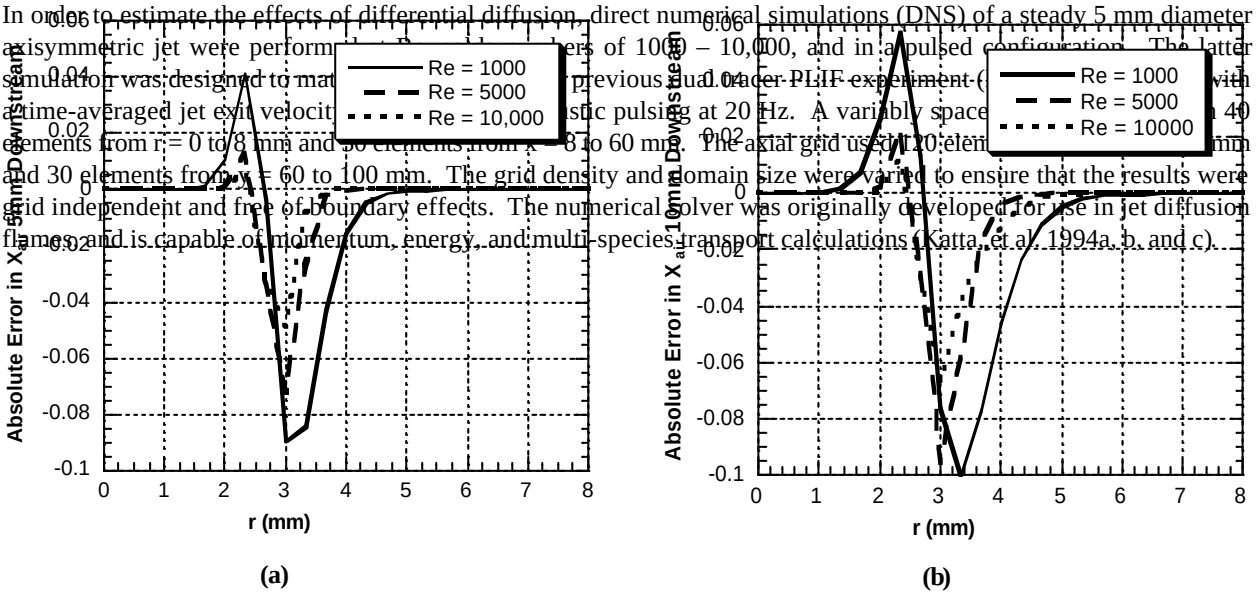

Figure 8. Absolute error in the mole fraction of air due to differential diffusion within the laminar diffusion layer of a 5 mm diameter jet calculated using a direct numerical simulation. Results are presented for different Reynolds numbers at (a) 5 mm downstream and (b) 10 mm downstream of the jet exit.

Figure 8 shows the DNS results of the non-pulsed jet at Reynolds numbers from 1000 – 10,000, and at two downstream locations. As expected, air diffuses toward the center of the jet, leaving excess regions of air on the jet side and depleted regions on the co-flow side. Also as expected, the differential diffusion error decreases with Reynolds number and increases with downstream distance. It is difficult to extrapolate such results, however, to turbulent regions where the relative large-scale and small-scale velocities and diffusion length scales are unknown. Furthermore, experimental data such as that shown previously in Fig. 7 cannot be reliably obtained in turbulent regions because of subresolution stirring.

Alternatively, Fig. 9 shows the results of a direct numerical simulation in the driven jet configuration, which provides a pseudo-turbulent flowfield in the form of interacting vortices. Differential diffusion errors were calculated using the differences in acetone and air concentration, and applying these differences to the 2-level model (Eq. 8) and the cold-chemistry model (Eq. 4). Since the DNS is incapable of producing subresolution stirring, the following error analysis is somewhat idealized. In general, errors due to differential diffusion are highest in the laminar diffusion layer of Row 1 in Fig. 9, followed by the vortex roll-up of Row 2, and are lowest for the vortex pairing of Row 3. This trend would indicate that differential diffusion errors may be fairly minimal within turbulent, interacting structures.

When comparing errors from the two-level model quenching corrections versus the cold-chemistry model, the results vary. The two-level model is slightly less accurate in the laminar diffusion layer of Row 1 where differential diffusion is quite high. At a mixed jet fluid fraction of about 0.95, for example, the error in the two-level model is about 10%, while the error from the cold-chemistry model is less than 2%. The reason for the superior performance

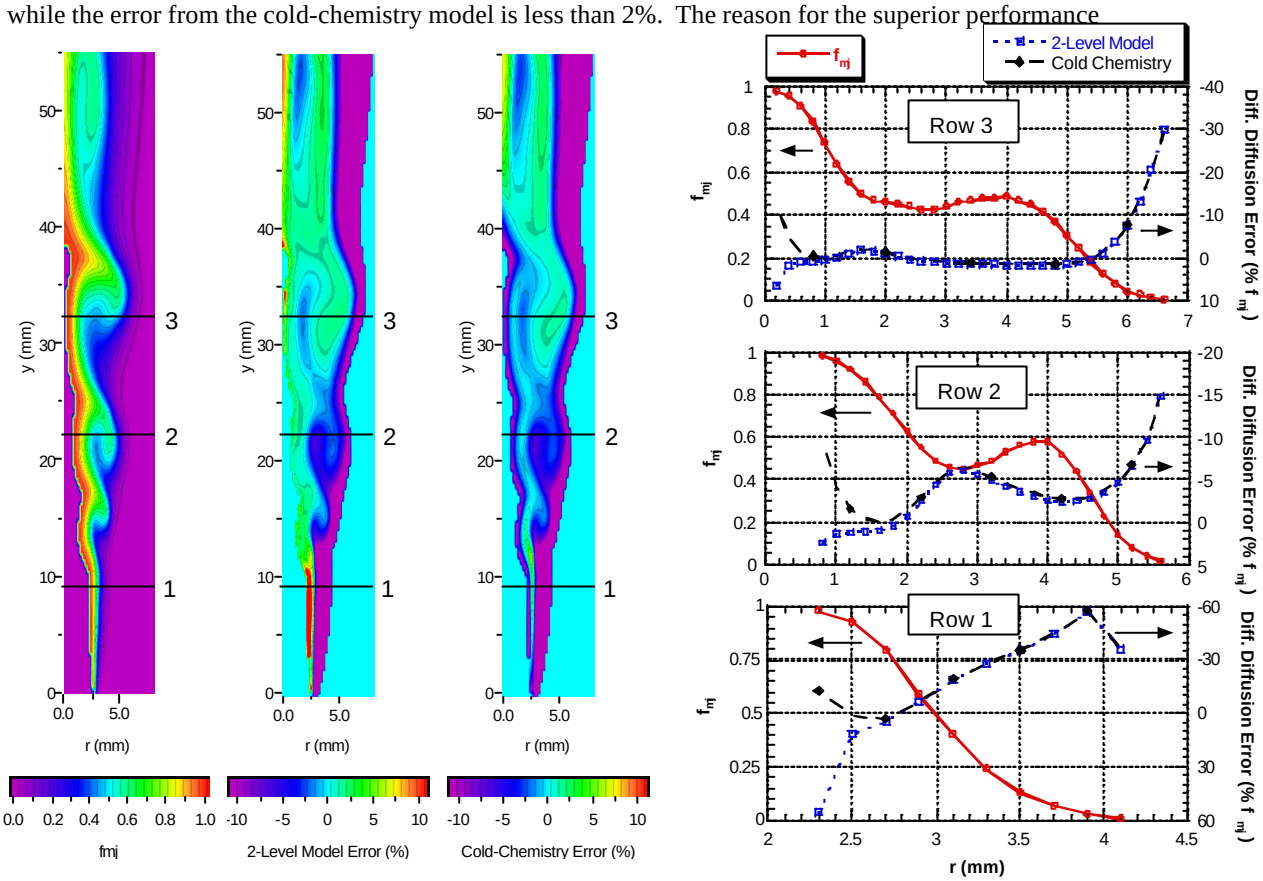

Figure 9. Mixed jet fluid fraction, f_{mj}, from a direct numerical simulation, and corresponding differential diffusion errors using the two-level model quenching corrections and the cold-chemistry model.

of the cold-chemistry model in the laminar diffusion layer can be understood by examining Eq. 4. Differential diffusion of air into a pixel element leads the measured value of x_{ac} to underestimate the amount of air, but also leads to extra quenching of NO, thereby reducing the measured vale of $x_{pure\ NO}$. These offsetting factors are on the same order of magnitude on the jet side of the laminar diffusion layer, and help reduce the cold-chemistry error in this region. The offsetting effect of differential diffusion, however, is limited to laminar regions

In Rows 2 and 3, for example, it is clear that the quenching corrections are slightly superior to the cold-chemistry model. In Row 3, for example, the two-level model results in an error of only 2% at a mixed jet fluid fraction of 0.95, compared with an error of 4% for the cold-chemistry model. This is indicative of reduced differential diffusion in the region of vortex interaction. Aside from this region of high mixed jet fluid fraction, the cold-chemistry model error is quite similar to that of the two-level model in all other regions of Row 3. The error for both models remains less than 2%, for example, in intermediate regions of Row 3, and is –8% for both models at a mixed jet fluid fraction of 0.05. The latter error, of course, is quite small in absolute terms.

The two-level model quenching corrections seem generally superior to the cold-chemistry model in regions of high mixed jet fluid fraction, but do not present any advantages in other regions of the flow. Because of the simplicity of the cold-chemistry model, therefore, it may be a better choice than the two-level model if uncertainties in the quenching environment are too large. Figure 10 illustrates an alternative experiment in which the nitrogen in the air co-flow is replaced with CO_2. Because CO_2 has a quenching cross-section that is almost six times that of oxygen, the two-level model in Fig. 10(a) more closely approximates the cold-chemistry model. The differential diffusion errors for both models are quite similar, even in the laminar diffusion layer as shown in Fig. 10(b), indicating that this would eliminate the need for the two-level model corrections. An added benefit is that the differential diffusion of CO_2 and acetone would be reduced by about 50% compared to that of acetone and air.

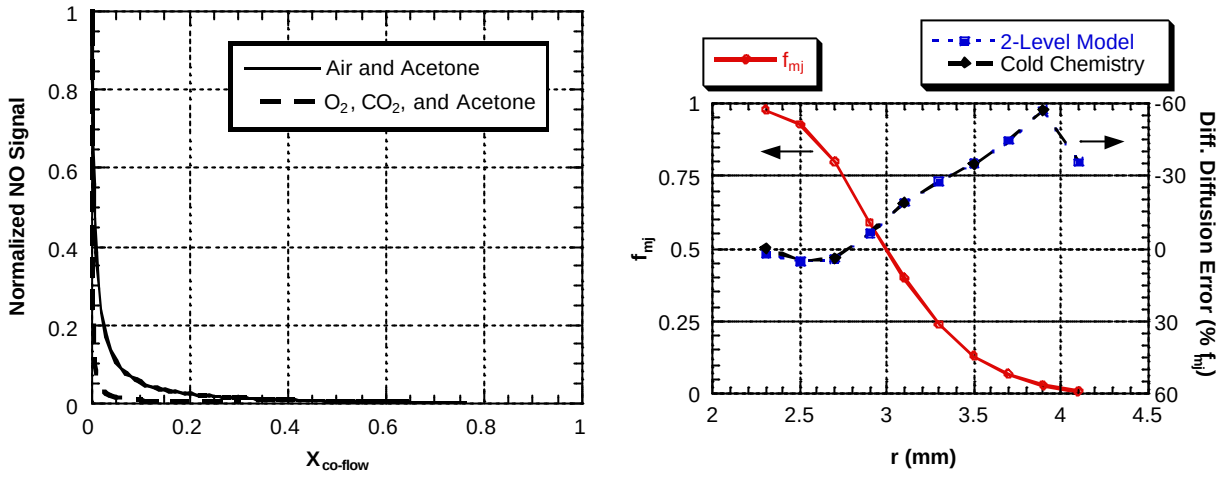

Figure 10. The effect of replacing nitrogen in the co-flow air with carbon dioxide on (a) the normalized NO fluorescence signal and (b) differential diffusion errors in the laminar diffusion layer (Row 1 of Fig. 9).

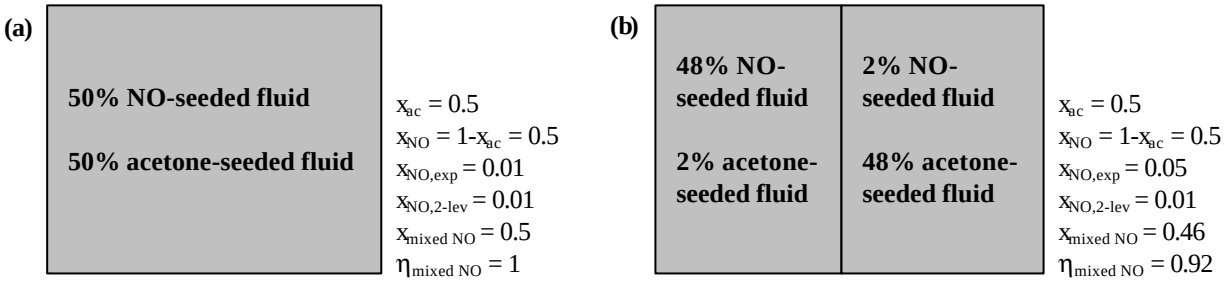

Figure 11. Sample calculations within a pixel element with equal parts NO and acetone-seeded fluid in which (a) the pixel is fully mixed throughout and (b) the pixel has a high subresolution concentration gradient.

7. FINITE SPATIAL RESOLUTION

As noted in Fig. 7, the differential diffusion error diminishes in the laminar diffusion layer at higher Reynolds numbers, but the error from finite imaging spatial resolution increases. To illustrate how finite imaging resolution can lead to errors in $x_{mixed\ NO}$ and $\eta_{mixed\ NO}$, it is useful to consider the example shown in Fig. 11. The pixel elements of Fig. 11(a) and (b) have the same overall amounts of NO- and acetone-seeded fluid, but in Fig. 11(a), almost all of the NO signal is quenched because it is molecularly mixed with 50% acetone-seeded air. The two-level model of Eq. 8 gives the correct values of $x_{mixed\ NO}$ and $\eta_{mixed\ NO}$. The pixel in Fig. 11(b), on the other hand, has high concentration gradients. Thus, the signal in the right half is almost entirely quenched since it is locally composed of 96% acetone-seeded fluid, but the signal in the left half has a residual NO signal of 0.1 x 50% = 5% since it is locally composed of only 4% acetone-seeded fluid. As a result, $x_{mixed\ NO} = 0.46$ and $\eta_{mixed\ NO} = 0.92$ from the two-level model, each of which have errors of about -8%. This phenomenon is most prominent on the NO-seeded side of turbulent shear layers, since these are regions that favor the presence of pixel elements like that of Fig. 11(b). If the imaging system had twice as many elements, it could fully resolve the concentration gradient and provide the correct measurements of $x_{mixed\ NO}$ and $\eta_{mixed\ NO}$. In a sense, Fig. 11(b) represents "false" subresolution stirring, since all of the fluid is actually mixed on the molecular level so, in fact, $\eta_{mixed\ NO} = 1$. On the other hand, pixel elements such as Fig. 7(b) can serve the same useful purpose as pixels with true subresolution stirring. That is, they mark locations in which the imaging system cannot adequately resolve the smallest diffusion length scales.

8. CONCLUSIONS

The simultaneous measurement of NO and acetone PLIF represents a significant advance in the study of molecular mixing in high-speed gaseous flows. The experimental and theoretical foundations of the technique were summarized, and its effectiveness at measuring subresolution molecular mixing was demonstrated. There are a number of considerations, however, that must be taken into account in order to obtain quantitative results, including careful image processing procedures, quenching corrections, differential diffusion, and imaging resolution. It is also important to recognize certain conditions, such as regions of low or high air concentration, in which it is difficult for the technique to ensure quantitative accuracy. This was demonstrated, in particular, with the use of direct numerical simulations. In investigations which have implemented the simultaneous NO and acetone PLIF technique, cumulative experimental uncertainties are typically about 5%, but can be as high as 20% in regions of low molecularly mixed NO-seeded fluid fraction (King et al. 1999, Meyer et al. 1999a,b). As an alternative to quenching corrections, which can incur uncertainties from a variety of sources, the choice of alternate tracer species could be used to improve the cold-chemistry approximation and eliminate the need for such corrections. It may also be possible to use tracer species that reduce the amount of differential diffusion.

ACKNOWLEDGMENTS

This work was supported by the National Science Foundation, Division of Chemical and Transport Systems, Grant No. CTS 94-23280, with Dr. R. E. A. Arndt and Dr. J. F. Foss as monitors. In addition, the authors would like to thank Dr. Vish Katta of Innovative Scientific Solutions, Inc. for providing the DNS codes used in this investigation.

REFERENCES

Breidenthal, R. (1981). "Structure in turbulent mixing layers and wakes using a chemical reaction," *J. Fluid Mech.* **109**, 1-24.

Clemens, N. T. and Paul, P. H. (1995). "Scalar measurements in compressible axisymmetric mixing layers," *Phys. Fluids* **7**, 1071-1081.

Dahm, W. J. A., Southerland, K. B. and Buch, K. A. (1991). "Direct, High Resolution, Four-Dimensional Measurements of the Fine Scale Structure of Sc >> 1 Molecular Mixing in Turbulent Flows," *Phys. Fluids A* **3**, 1115-1127.

Eckbreth, A. C. (1988), Laser Diagnostics for Combustion Temperature and Species, Abacus Press, Kent, United Kingdom.

Hansen, D. A. and Lee, E. K. C. (1975). "Radiative and nonradiative transitions in the first excited singlet state of symmetrical methyl-substituted acetones," *J. Chem. Phys.* **62**, 183-189.

Hanson, R. K. (1986). "Combustion diagnostics: planar imaging techniques," Twenty-first Symposium (International) on Combustion, The Combustion Institute, pp. 1677-1691

Island, T. C., Urban, W. D., and Mungal, M. G. (1996). "Quantitative scalar measurements in compressible mixing layers," AIAA Paper No. 96-0685, 34th AIAA Aerospace Sciences Meeting and Exhibit, Reno, Nevada.

Katta, V. R., Goss, L. P. and Roquemore, W. M. (1994a). "Effect of non-unity Lewis number and finite-rate chemistry on the dynamics of a hydrogen-air jet diffusion flame," *Combust. Flame* **96**, 60-74.

Katta, V. R., Goss, L. P. and Roquemore, W. M. (1994b). "Numerical Investigations of Transitional H_2/N_2 Jet Diffusion Flames," *AIAA J.* **32**, 84-94.

Katta, V. R., Goss, L. P. and Roquemore, W. M. (1994c). "Simulation of vortical structures in a jet diffusion flame," *International Journal of Numerical Methods for Heat and Fluid Flow* **4**, 413.

King, G. F., Dutton, J. C. and Lucht, R. P. (1999). "Instantaneous, quantitative measurements of molecular mixing in the axisymmetric jet near field," *Phys. Fluids* **11**, 403-416.

King, G. F., Lucht, R. P. and Dutton, J. C. (1997). "Quantitative dual-tracer planar laser-induced fluorescence measurements of molecular mixing," *Opt. Lett.* **22**, 633-635.

Koochesfahani, M. M., Dimotakis, P. E. and Broadwell, J. E. (1985). "A "Flip" Experiment in a Chemically Reacting Turbulent Mixing Layer," *AIAA J.* **23**, 1191-1194.

Lozano, A., Yip, B. and Hanson, R. K. (1992). "Acetone: a tracer for concentration measurements in gaseous flows by planar laser-induced fluorescence," *Exp. Fluids* **13**, 369-376.

Meyer, T. R., Dutton, J. C. and Lucht, R. P. (1999a). "Vortex interaction and mixing in a driven gaseous axisymmetric jet," *Phys. Fluids* **11**, 3401-3415.

Meyer, T. R., Dutton, J. C. and Lucht, R. P. (1999b). "Experimental Study of the Mixing Transition in a Gaseous Axisymmetric Jet," AIAA Paper No. 99-3585, 30th AIAA Fluid Dynamics Conference, Norfolk, Virginia.

Paul, P. H. and Clemens, N. T. (1993). "Sub-resolution flowfield measurements of unmixedness using electronic quenching of NO $A\,^2\Sigma^+$," *Opt. Lett.* **18**, 161.

Paul, P. H., Gray, J. A., Durant, J. L. and Thoman, J. W. (1994). "Collisional Quenching Corrections for Laser-Induced Fluorescence Measurements of NO $A\,^2S^+$," *AIAA J.* **32**, 1670-1675.

Seitzman, J. M., Miller, M. F., McMillin, B. K., Hanson, R. K., DeBarber, P. A., and Hess, C. F. (1994). "Multiple scalar planar fluorescence imaging for reacting flows," AIAA Paper No. 94-0228, 32nd AIAA Aerospace Sciences Meeting and Exhibit, Reno, Nevada.

Su, L. K. and Clemens, N. T. (1998). "The Structure of the Three-Dimensional Scalar Gradient in Gas-Phase Planar Turbulent Jets," AIAA Paper No. 98-0429, 36th AIAA Aerospace Sciences Meeting and Exhibit, Reno, Nevada.

Yip, B., Lozano, A. and Hanson, R. K. (1994). "Sensitized phosphorescence: a gas phase molecular mixing diagnostic," *Exp. Fluids* **17**, 16-23.

Yip, B., Miller, M. F., Lozano, A. and Hanson, R. K. (1994). "A combined OH/acetone planar laser-induced fluorescence imaging technique for visualizing combusting flows," *Exp. Fluids* **17**, 330-336.